

Superdeformed Band in Asymmetric $N > Z$ Nucleus, ^{40}Ar and High-Spin States in $A = 30 \sim 40$ Nuclei

Eiji IDEGUCHI,¹ Shinsuke OTA,¹ Tsuneyasu MORIKAWA,² Masumi OSHIMA,³
 Mitsuo KOIZUMI,³ Yosuke TOH,³ Atsushi KIMURA,³ Hideo HARADA,³
 Kazuyoshi FURUTAKA,³ Shoji NAKAMURA,³ Fumito KITATANI,³
 Yuichi HATSUKAWA,³ Toshiyuki SHIZUMA,³ Masahiko SUGAWARA,⁴
 Yutaka X. WATANABE,⁵ Yoshikazu HIRAYAMA⁵ and Makito OI⁶

¹*Center for Nuclear Study, The University of Tokyo, Wako 351-0198, Japan*

²*Department of Physics, Kyushu University, Fukuoka 812-8581, Japan*

³*Japan Atomic Energy Agency, Tokai, Ibaraki 319-1195, Japan*

⁴*Chiba Institute of Technology, Narashino 275-0023, Japan*

⁵*Institute of Particle and Nuclear Studies, KEK, Tsukuba 305-0801, Japan*

⁶*Institute of Natural Sciences, Senshu University, Tokyo 101-8425, Japan*

A rotational band with five cascade γ -ray transitions was newly found in ^{40}Ar . The deduced transition quadrupole moment of $1.45_{-0.31}^{+0.49}$ eb has demonstrated this band as having a superdeformed shape of $\beta_2 \sim 0.5$. The structure of the band was discussed in the framework of cranked Hartree-Fock-Bogoliubov calculations and the assignment of multiparticle-multihole configuration has been made.

§1. Introduction

After the systematic investigation of superdeformation in various mass regions,¹⁾ a new ‘island’ of superdeformed (SD) nuclei was found in the nuclear chart around $A \sim 40$ (i.e., ^{36}Ar ,²⁾ ^{40}Ca ,³⁾ and ^{44}Ti ⁴⁾). These $N = Z$ nuclei are magic and near magic systems whose ground states have a spherical shape. In order to produce the collective degrees of freedom necessary for the formation of SD states in these nuclei, cross-shell excitations involving both the sd and pf shells are necessary. SD shell structure in this mass region plays an important role to form such large deformed structures. Woods-Saxon single-particle diagram (see Fig. 4 of Ref. 3)) shows a SD gap at $\beta_2 \sim 0.6$ in $N = Z = 20$, which is associated with the SD band of ^{40}Ca ³⁾ with 8 particle 8 hole (8p-8h) configuration built on the third 0^+ state. Another SD gap at $\beta_2 \sim 0.5$ at $N = Z = 18$ is associated with the observed SD band in ^{36}Ar ²⁾ which is built on the second 0^+ state with 4p-4h configuration. The existence of many deformed gaps in this region may result in the SD structures at the excited 0^+ states and rotational bands built on such states are expected at high-spin levels. If such simple picture generally holds in this mass region, another SD structure in asymmetric $N > Z$ nucleus, ^{40}Ar , associated with the $Z = 18$ and $N = 22$ SD shell gaps will be present.

The presence of the SD band starting from the excited 0^+ level is another remarkable feature in this mass region. SD bands in the other mass region were found in much higher-spin regime ($\gtrsim 20\hbar$) and the observed lowest level of the band is supposed to lie ~ 3 MeV above the yrast line. In most cases, linking transitions

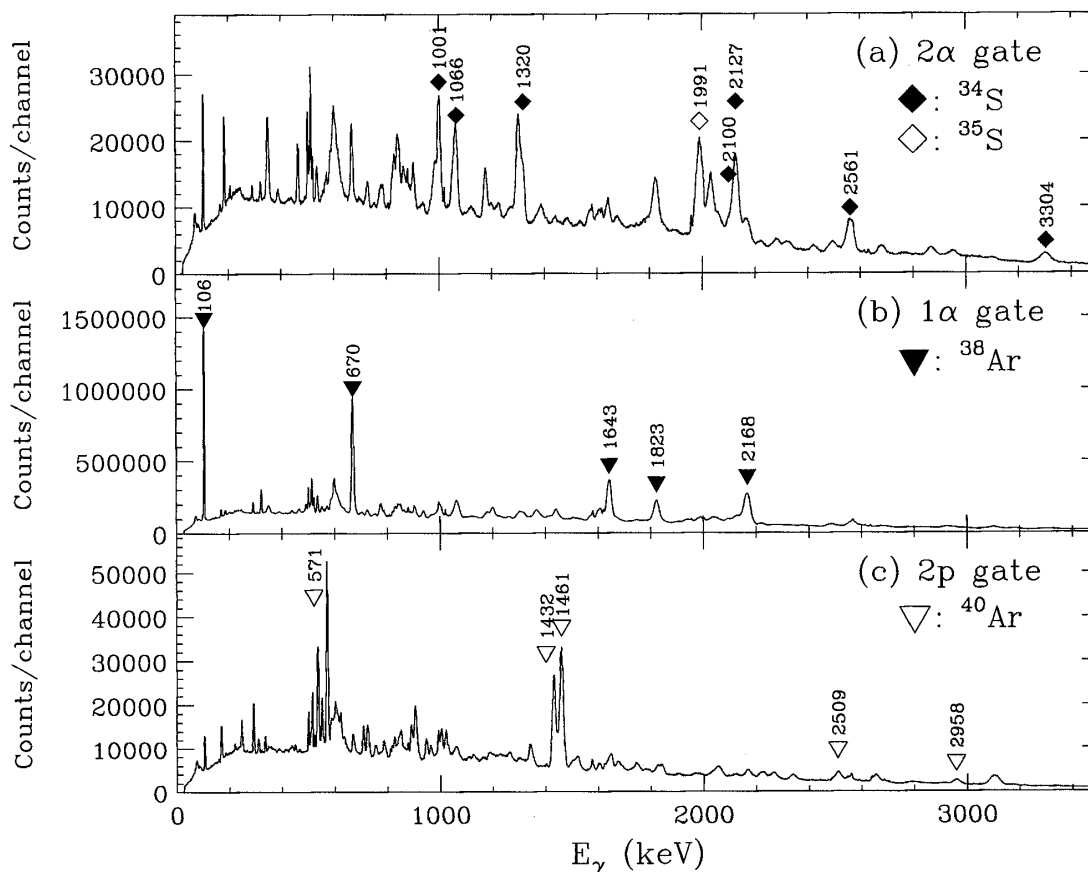


Fig. 1. Gamma-ray spectra created by gating on the number of hit of charged particles. Top panel corresponds to the 2 α gated spectrum, which corresponds to the S isotopes. Indeed, γ -ray peaks originated from $^{34,35}\text{S}$ (2 α 2n, and 2 α 1n channel, respectively) are clearly enhanced. Middle and bottom panel are 1 α and 2 protons gated spectrum, respectively. Similarly, γ peaks of ^{38}Ar (1 α 2n channel) and ^{40}Ar (2p2n channel) are also enhanced.

between the SD bands and low-lying normal deformed bands were not found, which makes it difficult to firmly identify the excitation energy and the spin-parity of the SD band. On the contrary, SD bands observed in $A \sim 40$ region are all linked to the low-lying levels and bands are ranging from 0^+ to 16^+ .

In order to investigate SD structures predicted in ^{40}Ar and neighboring isotopes, we have performed an in-beam γ -ray spectroscopy.

§2. Experiment and data analysis

Excited states of ^{40}Ar were previously studied by proton- γ coincidence measurements in the $^{37}\text{Cl}(\alpha, p\gamma)$ reaction.⁵⁾ The coexistence of spherical and deformed states was suggested and the $K^\pi = 0^+$ rotational band up to the 6^+ level, which decays to the low-lying spherical levels, was assigned. In addition, (8^+) level was proposed as a member of the rotational band based on the similarity to the band structure in ^{42}Ca . However, in their measurement mutual coincidence relation of the γ transitions couldn't be confirmed by the $\gamma - \gamma$ coincidence and higher spin levels weren't populated.

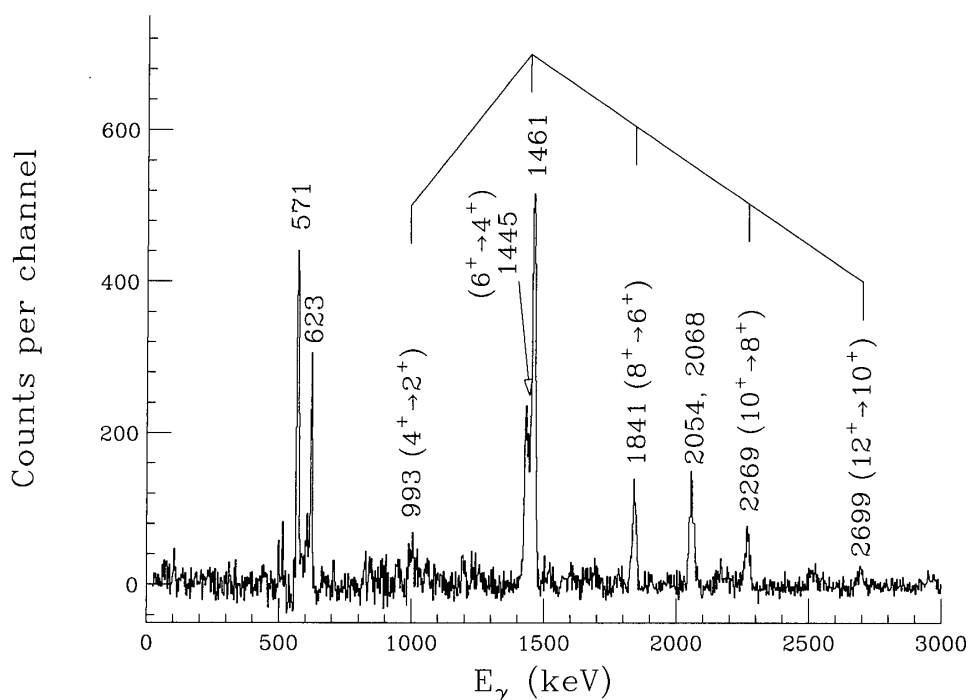


Fig. 2. Gamma-ray energy spectrum of SD band in ^{40}Ar created by gating on in-band transitions. Transitions of the SD band are connected by solid line and γ -ray energy of each transition is labeled on the peak. Spin and parity of the initial and final level of each transition is shown in the parentheses.

In order to study higher-spin levels, a heavy-ion induced fusion-evaporation reaction, $^{26}\text{Mg}(^{18}\text{O}, 2\text{p}2\text{n})^{40}\text{Ar}$ at 70 MeV, was employed. Two stacked self-supporting ^{26}Mg foils of 0.5 mg/cm^2 for each, were bombarded by ^{18}O ions delivered from the tandem accelerator at the Japan Atomic Energy Agency (JAEA). Gamma rays were measured by the GEMINI-II array⁶⁾ consisting of 16 HPGe detectors with BGO Compton suppression shields. Charged particles evaporating from the compound nucleus were detected by the Si-Ball, a 4π array of ΔE Si detectors of $170 \mu\text{m}$ thick.⁷⁾ A VME-based data acquisition system of CNS was used and it was triggered by the events of more than two Compton-suppressed Ge firing in coincidence with the Si-Ball signals. By gating on the number of hits of charged particles, data were sorted off-line into E_γ - E_γ correlation matrices for corresponding evaporation channels. Figure 1 shows γ -ray spectra created by gating on (a) 2 α particles-, (b) 1 α particle-, and (c) 2 protons-hitting events. As shown in the figure, γ rays associated with ^{40}Ar were clearly enhanced by gating on two protons.

In the analysis of E_γ - E_γ correlation matrices, the RADWARE software package⁸⁾ was used. By gating on the known transitions in ^{40}Ar , a number of high-spin levels were newly identified and a rotational band with five γ -ray transitions ranging from 2^+ to 12^+ states was identified as shown in Fig. 2. Based on the coincidence relations and the multiplicities of γ transitions deduced by the DCO ratio analysis, the assignment of spin and parity has been made. The previously assigned deformed band was extended up to $J^\pi = (12^+)$ state at 11769 keV.

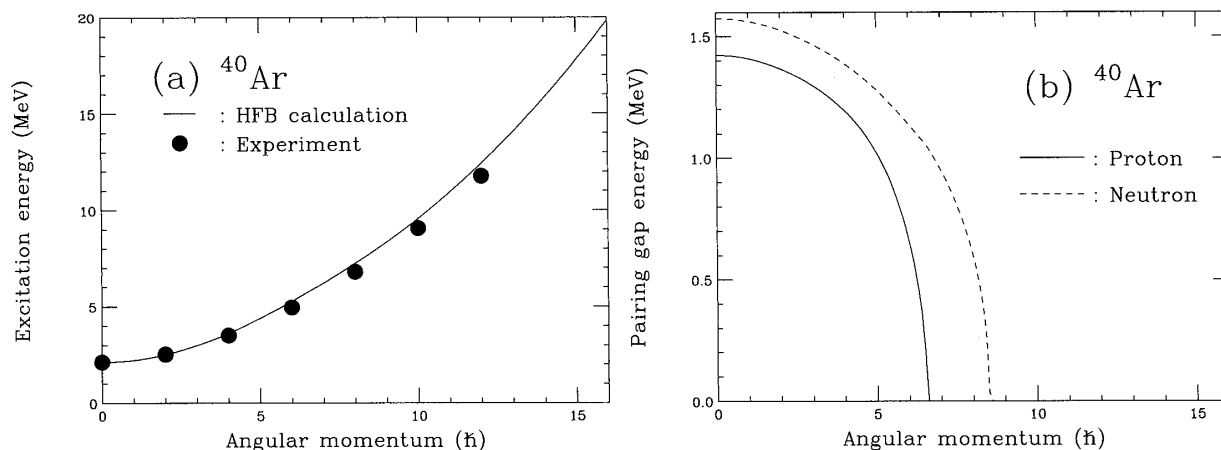


Fig. 3. Excitation energy (left panel) and pairing gap energy (right panel) by the HFB calculation. Calculated excitation energy was normalized to the experimental value at spin $0 \hbar$ (i.e. 2.121 MeV).

§3. Results and discussion

In order to estimate the deformation of the band, transition quadrupole moment, Q_t was deduced by the lifetime analysis based on the residual Doppler shift of the γ -ray peaks.⁹⁾ The deduced value of $Q_t = 1.45^{+0.49}_{-0.31}$ eb represents a quadrupole deformation of $\beta_2 \sim 0.5$ for an assumed axially symmetric rigid rotor. The large β_2 value favorably compares with those for SD bands in ^{40}Ca (≈ 0.58) and ^{36}Ar (≈ 0.45).

In order to understand the high-spin structure in ^{40}Ar , cranked Hartree-Fock-Bogoliubov (HFB) calculations with the P + QQ force¹⁰⁾ were performed. The model space of the full sd - fp shell with the $g_{9/2}$ was used and the evolution of the shape was treated in the self-consistent manner. The calculation showed that the deformation of $\beta_2 = 0.57$ at $J = 0\hbar$ gradually decreases to 0.45 at $J = 12\hbar$ while γ deformation remains to be almost zero throughout this angular momentum range. This agrees with the experimental Q_t value within the error bars.

The occupation numbers of each orbital were also calculated. At the second 0^+ state, calculation indicates that 2 protons and 4 neutrons are occupied in fp shell while 2 neutrons are in fp shell and 2 holes in sd shell at the ground state. This corresponds to the 4p-4h excitation relative to the ground state.

In Figure 3, calculated excitation energies (a) as well as the pairing gap energies (b) were plotted as a function of angular momentum. In the plot, calculated excitation energy curve was normalized to that of experimental value at spin 0 (i.e. 2.212 MeV). Overall trend of the high-spin behavior of the excitation energy was reproduced fairly well. As shown in the figure, pairing gap energy becomes 0 around spin $8 \hbar$ for both proton and neutron.

For the comparison of high-spin behavior of the SD band in ^{40}Ar with those in ^{40}Ca and ^{36}Ar , so called backbending plot is shown in Fig. 4. The kinematical moment of inertia, $J^{(1)}$, corresponds to the gradient. As can be seen in the figure, the $J^{(1)}$ of ^{40}Ar is comparably large as those of ^{40}Ca and ^{36}Ar . Note that, in contrast to the ^{36}Ar , no backbending is seen for ^{40}Ar at least up to $J^\pi = 12^+$. This suggests that

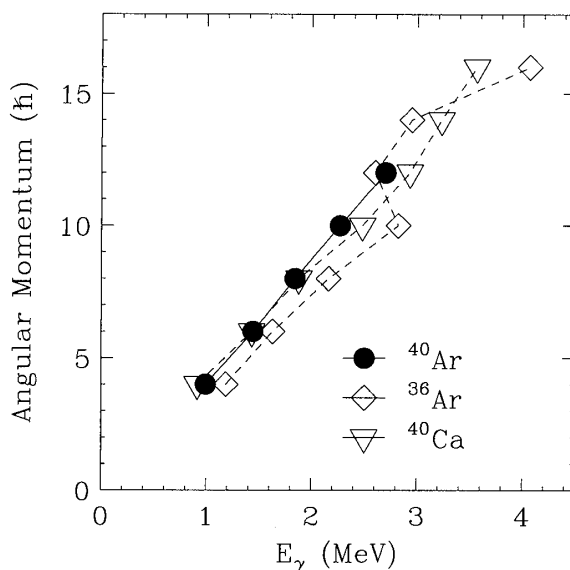


Fig. 4. Backbending plot of SD bands in ^{36}Ar , ^{40}Ar and ^{40}Ca .

an addition of four neutrons to ^{36}Ar leads to a significant change in the high-spin yrast structure.

According to the HFB calculation, the behavior of the proton occupation number of ^{40}Ar is similar to that of ^{36}Ar against the increase of angular momentum. As to neutrons, on the other hand, a clear difference is seen from the ^{36}Ar case as the angular momentum increases. The occupation number in $\nu f_{7/2}$ orbital is almost constant (~ 3) for ^{40}Ar , which is 1.5 larger than that for ^{36}Ar . In the case of ^{36}Ar , a structural change involving the sharp backbending is caused by excitation from $p_{3/2}$ to $f_{7/2}$ for both protons and neutrons at spin $\sim 8\hbar$. As to neutrons in ^{40}Ar , this excitation happens from $p_{3/2}$ to many other orbitals because of the rise of neutron Fermi surface. Many $\Omega = 1/2$ states are vacant in ^{36}Ar when the excitation from $p_{3/2}$ to $f_{7/2}$ happens. On the contrary, neutron $\Omega = 1/2$ states in ^{40}Ar are already filled, which leads to the suppression of the rotational alignment; simultaneous alignment of $f_{7/2}$ protons and neutrons does not occur. This may explain the non observation of backbending in ^{40}Ar .

In order to find the dynamical behavior of the SD band at high-spin states, experimental and calculated kinematical ($J^{(1)}$) and dynamical ($J^{(2)}$) moments of inertia for ^{40}Ar were plotted in Fig. 5 as a function of rotational frequency. As shown in the figure, HFB calculations reproduced both magnitude and behaviors of $J^{(1)}$ and $J^{(2)}$ values rather well. At the rotational frequency of 0.8 MeV, which corresponds to spin $8\hbar$, $J^{(2)}$ moment of inertia drops. This trend also appears in the calculation as a bump around 0.9 MeV, which corresponds to the point where the pairing gap energy disappears. The change of the moment of inertia reflects this attenuation of pairing effect and may imply the pairing phase transition from super to normal conducting phase. Similar trend also appeared in the HFB calculation of ^{36}Ar and ^{40}Ca ¹⁰⁾ and it is also observed experimentally in the rotational band of the neighboring isotope, ^{42}Ca .¹²⁾ These results indicate that this attenuation of pairing

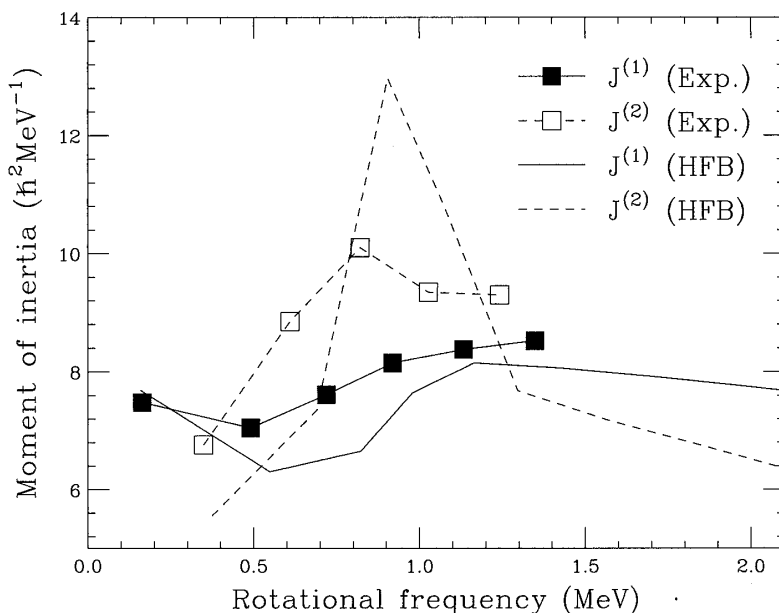


Fig. 5. Experimental and calculated kinematical ($J^{(1)}$) and dynamical ($J^{(2)}$) moment of inertia of ^{40}Ar as a function of rotational frequency.

generally appear in this mass region and it will be further investigated.¹²⁾

§4. Summary

An SD band has been identified in ^{40}Ar . The transition quadrupole moment $Q_t = 1.45_{-0.31}^{+0.49}$ eb deduced from the lifetime analysis supports a picture of the SD shape for this band. The character of the SD band is well explained by cranked HFB calculations. The onset of superdeformation in ^{40}Ar suggests the persistence of SD shell gap at $Z = 18$, $N = 22$ in the neutron-rich $A \sim 40$ region.

Acknowledgements

The authors are grateful to the crew of JAEA tandem accelerator for providing the ^{18}O beam. E. I. thanks Prof. Matsuyanagi, Prof. Shimizu, and Dr. Inakura for valuable discussions.

References

- 1) B. Singh, R. Zywina and R. B. Firestone, Nucl. Data Sheets **97** (2002), 241.
- 2) C. E. Svensson et al., Phys. Rev. Lett. **85** (2000), 2693.
- 3) E. Ideguchi et al., Phys. Rev. Lett. **87** (2001), 222501.
- 4) C. D. O'Leary et al., Phys. Rev. C **61** (2000), 064314.
- 5) E. Bitterwolf et al., Z. Phys. A **313** (1983), 123.
- 6) M. Oshima et al., J. Radio. Nucl. Chem. **278** (2008), 257.
- 7) T. Kuroyanagi et al., Nucl. Instrum. Methods Phys. Res. A **316** (1992), 289.
- 8) D. C. Radford, Nucl. Instrum. Methods Phys. Res. A **351** (1995), 297.
- 9) B. Cederwall et al., Nucl. Instrum. Methods Phys. Res. A **354** (1995), 591.
- 10) M. Oi, Phys. Rev. C **76** (2007), 044308.
- 11) E. Ideguchi et al., Phys. Lett. B **686** (2010), 18.
- 12) E. Ideguchi et al., to be published.